Design, synthesis and biological evaluation of a novel [^{18}F]AlF-H_3RESCA-FAPI radiotracer targeting fibroblast activation protein*

Qingyu Zhang,[1,2] Zhoumi Hu,[1] Haitao Zhao,[1] Fuqiang Du,[1] Chun Lv,[1] Tukang Peng,[1] Yukai Zhang,[1,2] Bowu Zhang,[2,†] Jianjun Liu,[1,‡] and Cheng Wang[1,§]

[1]*Department of Nuclear Medicine, Institute of Clinical Nuclear Medicine, Renji Hospital, School of Medicine, Shanghai Jiao Tong University, Shanghai 200127, China*

[2]*MOE Key Lab of Resource Chemistry, Joint International Research Laboratory of Resource Chemistry of Ministry of Education, Shanghai Key Laboratory of Rare Earth Functional Materials, and Shanghai Frontiers Science Centre of Biomimetic Catalysis, College of Chemistry and Materials Science, Shanghai Normal University, Shanghai 200234, China*

Fibroblast activation protein (FAP) is widely utilized in nuclear medical imaging and cancer diagnosis and treatment. Some small molecule FAP inhibitors (FAPIs) are used to develop diagnostic and therapeutic agents targeting FAP by conjugating the different radionuclides. However, ^{18}F-labeled FAPIs require further expansion. In this study, We attempted to label FAPI with ^{18}F by H_3RESCA chelator group. The efficacy and pharmacokinetics of H_3RESCA-FAPI were predicted and evaluated by molecular docking, ADMET properties, affinity test, labeling, positron emission tomography (PET) imaging with U87MG model mice and *in vitro* biological distribution. The excellent labelling conjugation of H_3RESCA-FAPI and aluminum fluoride ([^{18}F]AlF) in mild conditions, high affinity for FAP, rapid clearance *in vivo*, effective visualization of tumor tissue and high target and nontarget uptake ratio indicate that [^{18}F]AlF-H_3RESCA-FAPI is a potential PET imaging tracer targeting FAP. However, the extremely high liver and intestine uptake illustrate further structural modifications are necessary to optimize its pharmacokinetics and improve imaging quality.

Keywords: H_3RESCA Chelator, Fibroblast Activation Protein Inhibitor, Fluorine-18, Positron Emission Tomography

I. INTRODUCTION

Tumor microenvironment (TME), including fibroblasts, myeloid-derived suppressor cells (MDSCs), macrophages, lymphocytes, the extracellular matrix (ECM) and intertwined blood vessels constructed by endothelial cells and pericytes [1]. These stromal cells tightly interact with cancer cells, creating a supportive environment for tumor growth.Among these, cancer-associated fibroblasts (CAFs) play a crucial role in tumor progression by contributing to processes such as tumorigenesis, neoangiogenesis, metastasis, immunosuppression, and drug resistance [2, 3]. Fibroblast activation protein (FAP), a type II transmembrane serine protease belonging to the dipeptidyl peptidase 4 family with both dipeptidyl peptidase and endopeptidase activity [4], is overexpressed on CAFs in more than 90% of epithelial carcinomas [5–8].

Therefore, FAP is considered a promising target for both tumor imaging and therapy. In 2014, UAMC-1110 (Fig. 1(A)) was identified as the most potent and selective small molecule inhibitor of FAP [9, 10]. Since then, some classic UAMC-1110-based PET tracers have been developed [11–13], such as [^{68}Ga]Ga-DOTA-FAPI-04 (Fig. 1(B)) and [^{18}F]AlF-NOTA-FAPI-42 (Fig. 1(C)).

Initially, [^{68}Ga]Ga-DOTA-FAPI-04 garnered the majority of attention within the FAPI-diagnostics field [14]; however, current research is also focusing on ^{18}F-labeled FAPIs due to the excellent spatial resolution theoretically obtained by ^{18}F-PET imaging [15] and the relatively long half-life of ^{18}F ($t_{1/2}$ = 109.8 min, compared with $t_{1/2}$(^{68}Ga) = 67.7 min). Furthermore, the limited availability of ^{68}Ga, which must be produced in relatively small batches through ^{68}Ge/^{68}Ga generators, contributes to the growing interest in ^{18}F-labeled FAPIs. On the contrary, ^{18}F can be mass-produced in cyclotron or transported to PET imaging center which lacking radionuclide production capacity [16, 17].

The labeling techniques for ^{18}F can be categorized into two groups: nucleophilic ^{18}F-derivatives generated by various substitution reactions [15, 18, 19], and the utilization of aluminum fluoride ([^{18}F]AlF) for radiolabeling via coordination chemistry [20]. The method of using [^{18}F]AlF labeling has been expanding, and a series of different chelator groups have achieved great success, such as NOTA, NODA, NODAGA, 2-AMPTA, DTPA, most of these require certain requirements for equipment [21].

Recently, the H_3RESCA has been widely used in ^{18}F labeling of antibodies because of its mild reaction conditions and straightforward labeling process [22, 23], which has piqued our interest. Our research aims to utilize H_3RESCA for the labeling of small molecules with ^{18}F, using FAPI as an example to broaden the potential applications of FAPI in nuclear medicine (Fig. 1(D)).

* Supported by the National Key Research and Development Program of China (No. 2021YFF0701900 and No. 2020YFA0909000), the Interdisciplinary Program of Shanghai Jiao Tong University (No. ZH2018QNB20) and the construction project of Shanghai Key Laboratory of Molecular Imaging(18DZ2260400) (No. KFKT-2024-27).

† Corresponding author, zhangbowu@shnu.edu.cn

‡ Corresponding author, nuclearj@163.com

§ Corresponding author, wangch628@163.com

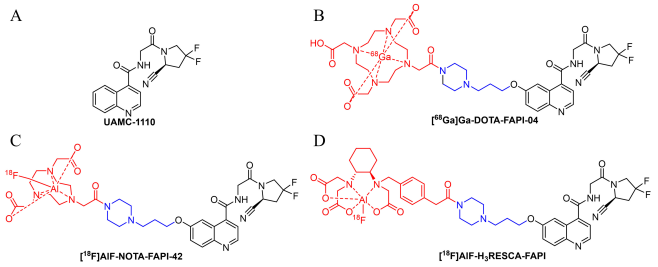

Fig. 1. The structures of UAMC-1110 (A), [^{68}Ga]Ga-DOTA-FAPI-04 (B), [^{18}F]AlF-NOTA-FAPI-42 (C) and [^{18}F]AlF-H_3RESCA-FAPI (D). The blue part is the linker, the red part is the chelator group, and the black part is FAPI pharmacophore.

II. MATERIAL AND METHODS

A. General

Except as indicated, compound 1 and compound 2 were procured from TanzhenBio (Nanchang, China), and other chemicals and reagents were procured from Merck (Shanghai, China) and used without additional purification. Characterization of synthesized compounds was performed using LC-MS on an Infinity Lab mass spectrometer equipped with an Agilent 1260 series HPLC system and an Extend-C18 column (50 mm $\times$ 2.1 mm, 1.8 μm), monitores at a UV wavelength of 254 nm. Radioisotope $^{18}F^-$ was produced in a medical cyclotron (HM-10, Sumitomo Heavy Industries Ltd., Tokyo, Japan) via the ^{18}O(p, n)^{18}F reaction. Quality control of the radiotracers was conducted using HPLC with a C18 column (C18-TH, 5μm, 100Å, 150mm $\times$ 4.6mm, Morhchem Technologies Inc., United States) and a 1260 Quat pump VL, a 1260 DAD VL detector, a 1260 Vialsampler, and a γ-detector for radioactivity measurement (Eckert and Ziegler, United States). The mobile phase composition of water and acetonitrile was adjusted according to the specific compounds. Radioactivity measurements were taken with a CRC-55T activity meter (The China National Nuclear Corporation, Beijing, United States).

B. Molecular Docking

Three-dimensional structures of DOTA-FAPI-04, NOTA-FAPI-42 and H_3RESCA-FAPI were constructed using Chem3D 20.0 (PerkinElmer). The resultant mol2 files were converted to .pdb format with PyMol 2.6.0. The target protein (PDB ID: 1Z68) underwent preparation for docking by adding hydrogen atoms with AutoDockTools 1.5.7 (The Scripps Research Institute). A docking grid, encompassing the catalytic site of FAPα, was defined. This grid was centered around the catalytic triad—Ser^{624}, Asp^{702}, and His^{734}—using AutoGrid 4.0, which set the grid dimensions at 24 $\times$ 24 $\times$ 24 Å^3 and a grid spacing of 1.000 Å, to ensure comprehensive coverage of the catalytic site. The coordinates for the grid box center were established at x = 25.071 Å, y = 10.676 Å, and z = 25.618 Å. Molecular docking, carried out with Autodock Vina 1.1.2, evaluated the influence uof various chelator groups on the binding affinity of FAPI-4 to FAP. Each compound underwent three independent docking simulations. The lowest-energy conformation from each set of runs, as identified by Autodock Vina, was selected for visualization with PyMol 2.6.0.

C. ADMET Profiling Studies

The absorption, distribution, metabolism, excretion and toxicity (ADMET) properties of FAPI-based ligands were predicted using the ADMETlab 3.0 web tools, which facilitate a comprehensive ADMET analysis. Ligand structures, described by their Simplified Molecular Input Line Entry System (SMILES) representations, were input into the platform to generate 2D structural files. This enabled ADMETlab 3.0 to compute and evaluate essential ADMET parameters effectively. Notably, the SMILES strings for two specific ligands were generated with ChemDraw 20.0 and are detailed in Supplementary Texts S1 and S2.

D. Chemistry

2,2'-(((1R,2R)-2-((carboxymethyl)(4-(2-(4-(3-((4-((2-((S)-2-cyano-4,4-difluoropyrrolidin-1-yl)-2-oxoethyl)carbamoyl)quinolin-6-yl)oxy)propyl)piperazin-1-yl)-2-oxoethyl)benzyl)amino)cyclohexyl)azanediyl)diacetic acid (3).

Compound 1 (50 mg, 103 μmol) was dissolved in DMSO (4 mL), followed by the addition of compound 2 (77 mg, 131 μmol) and triethylamine (Et_3N, 100 μL, 719 μmol). The mixture was stirred at room temperature (20 °C) for 4 hours and then concentrated under reduced pressure. Purification was achieved using semi-preparative HPLC with a COSMOSIL 5C18-MS-II column (120 Å, 5 μm, 250 $\times$ 10.0 mm) and a gradient elution of acetonitrile/water (0.1% TFA) initiated at 16/84 (v/v) for 20 minutes at a flow rate of 2 mL/min. The solvent was removed under reduced pressure to yield compound 3 as a white powder (32.2 mg, 34.6%). LC-MS (ESI) analysis showed a molecular ion peak at m/z = 904.8 $[M+H]^+$.

E. Binding Affinity Measurement

In order to determine the binding kinetics between ligands and human FAP protein (10464-H07H Sino Biological), the Biacore SPR interaction study was conducted. The binding affinity is expressed by the equilibrium dissociation constant (K_D) (M), which is calculated from the values of the measured binding rate constant (k_a) ($M^{-1}\,s^{-1}$) and dissociation rate (k_d) (s^{-1}).

F. Radiochemistry and Quality Control

$^{18}F^-$ was loaded onto an activated QMA ion exchange column (Waters GmbH, Germany), which had been previously eluted with 1 mL of saline and air-dried. The column containing $^{18}F^-$ was subsequently eluted with 1 mL of saline to obtain a $Na^{18}F$ solution.

Reaction conditions were screened using five different pH buffers: a NaHP buffer at pH 6.0 (0.2 M) and a sodium acetate buffer ranging from pH 4 to 5.5 (0.2 M). For the reactions, 100 μL of $Na^{18}F$ solution (370 MBq) and 12 μL of $AlCl_3$ solution (1.28 mM, prepared in 0.2 M buffer solution) were added to a reaction vial. The mixture was incubated at room temperature for 5 min. Subsequently, 300 μL of buffer solution at varying pH values and 200 μL of H_3RESCA-FAPI solution (0.1 mg/mL, prepared in deionized water) were added, and the mixture was allowed to react for 15 minu at room temperature. The radiolabeling yields across different pH conditions were quantified by HPLC.

Utilizing the pH buffer that yielded the highest radiolabeling efficiency, 10 μL of $Na^{18}F$ solution (37 MBq) and variable volumes of $AlCl_3$ solution (either 12 or 12.4 μL, 1.07 mM, prepared in the selected buffer) were added to a reaction vial and incubated at room temperature for 5 min. This was followed by the addition of 200 μL of H_3RESCA-FAPI solution (0.1 mg/mL, prepared in the selected buffer) and 300 μL of the same buffer. The reaction proceeded for 15 min at room temperature. Radiolabeling efficiencies were then calculated by HPLC, analyzing different $AlCl_3$ to ligand molar ratios (0.58 or 0.60).

In a subsequent experiment, the selected volume of $AlCl_3$ was added to a reaction flask along with 100 μL of $Na^{18}F$ solution (185 MBq) and incubated at room temperature for 5 min. Different volumes of H_3RESCA-FAPI solution (200, 500, or 1000 μL, 0.1 mg/mL, prepared in the selected buffer) were then introduced, maintaining the same volume with the selected buffer. The reaction was sustained for 15 min at room temperature. Radiolabeling yields for varying ligand masses (20, 50, or 100 μg) were determined by HPLC.

The purification protocol for the Sep-Pak Light C18 column involved first eluting the reaction solution with 5 mL of pure water through the activated column. The purified product was then collected into an aseptic vacuum bottle containing 1 mL of 50% ethanol solution, followed by the addition of 4 mL saline, rendering the preparation ready for use. For HPLC analysis, the mobile phase consisted of an aqueous solution containing 0.10% trifluoroacetic acid (Phase A) and acetonitrile (Phase B). An isocratic elution was employed, with a mobile phase consisting of 18% Phase B, maintained constant throughout the analysis. The flow rate was set at 1 mL/min. UV detection was performed at a wavelength of 254 nm.

G. Partition Coefficient

Radiotracers [^{68}Ga]Ga-DOTA-FAPI-04 and [^{18}F]AlF-H_3RESCA-FAPI (0.37 MBq, about 50 μL) was added to tubes containing n-octanol/PBS-mixture (1 mL, 1:1). The mixture was vortexed vigorously for 5 min at ambient temperature, and then centrifuged for five min at 8,000 rpm. In each phase, three samples (each 50 μL) was removed and measured in γ-counter (PerkinElmer). The partition coefficient was expressed as Eq. (1) (n = 3).

$$logD_{7.4} = log_{10}^{\frac{\mathrm{CPM}_{n-\mathrm{octanol}}}{\mathrm{CPM}_{\mathrm{PBS}}}}, \quad (1)$$

H. *In Vitro* and *In Vivo* Stability

[^{18}F]AlF-H_3RESCA-FAPI (10 MBq) in a mixture of ethanol and water was added to PBS (600 μL) or FBS (GE Healthcare, Chicago, IL, USA) (600 μL) and incubated at 37°C for 2 hours. And then, a sample of PBS or FBS (100 μL) was injected into the HPLC system for analysis. At 60 min post-injection of [^{18}F]AlF-H_3RESCA-FAPI (37 MBq/mouse), the mice were sacrificed. The urine was then collected and analysed with HPLC directly.

I. Pharmacokinetics In Normal Mice

The distribution of [^{18}F]AlF-H_3RESCA-FAPI (0.93 MBq) in blood was assessed at 1, 2, 5, 10, 20, 30, 60, 90, 120 min using normal mice. The mice (n = 3 in each group) were adopted the blood at the selected time. All the collected blood were quickly removed and weighed, and the radio activity was counted using a γ-counter and the results were expressed as percentage of injected dose per gram of tissue (%ID/g).

J. PET Imaging

U87MG tumor-bearing mice (n=3 per group) underwent PET imaging using an IRIS micro-PET/CT scanner (inviscan SAS, Strasbourg, France). Mice were anesthetized and positioned prone for the scans. Static PET images were acquired at 10, 30, 60, 90, and 120 min post-injection of [^{18}F]AlF-H_3RESCA-FAPI (4-6 MBq/mouse). For the blocking study, [^{18}F]AlF-H_3RESCA-FAPI was co-injecteded with unlabeled DOTA-FAPI-04 (0.5 mg/mouse), followed by a 1-hour static PET scan. The PET data were reconstructed using a three-dimensional ordered-subset expectation maximization (3D-OSEM) algorithm, which incorporates a Monte Carlo simulation for accurate modeling of the detector response. The reconstructed images were analyzed using Avatar 1.2 software (Pingseng China) for semi-quantitative assessment.

K. Biodistribution Studies

The biodistribution of [^{18}F]AlF-H_3RESCA-FAPI (4.32–5.45 MBq) was evaluated in athymic nude mice bearing U87MG xenografts at 1 hour post-injection (p.i.).

A subset of mice received a concurrent injection of the radiotracer and the competitor DOTA-FAPI-04 (0.5 mg per mouse) to assess blocking effects. At 60 min p.i., the mice (n=3 per group) were euthanized, and selected organs, tumors, and blood were harvested, weighed, and measured for radioactivity using a γ-counter. The results were expressed as %ID/g.

L. Immunohistochemical Staining

U87MG tumor tissues were harvested post-euthanasia and processed into paraffin-embedded sections for immunohistochemical analysis. Sections underwent deparaffinization in xylene and rehydration through graded ethanol. Antigen retrieval was performed, followed by overnight incubation with a rabbit polyclonal anti-FAP primary antibody (1:50, AF0739, Affinity) at 4°C. After rinsing, sections were incubated with a goat anti-rabbit secondary antibody (PV-9000, ZSGB-BIO) for 1 hour at room temperature. FAP expression was visualized using diaminobenzidine (DAB), counterstained with hematoxylin, dehydrated, cleared, and mounted. Positive staining was assessed and photographed under a microscope.

M. Statistical Analysis

Quantitative data are expressed as mean ± standard deviation (SD). The statistical significance between 2 independent groups was determined by the student t-test. A p-value of less than 0.05 was considered statistically significant. All statistical analyses were performed using GraphPad Prism version 8.0.1 (Graph Software, Inc).

III. RESULTS AND DISCUSSION

A. Docking Simulations

Molecular docking simulations were conducted to elucidate the interactions between FAPI-based ligands and the FAP enzyme, with the results depicted in Fig. 2 demonstrating that the introduction of this innovative chelating agent group enhanced the interaction. Specifically, H_3RESCA-FAPI exhibited a wider range of interactions with amino acid residues, including His^{734}, Ser^{624}, Arg^{123} and Tyr^{656}, Glu^{203}, compared to DOTA-FAPI-04, which primarily interacted with Ser^{624}, His^{734} and Arg^{123}, and NOTA-FAPI-42, which interacted with Glu^{203}, Tyr^{541}, Gln^{547} and Arg^{550}. These interactions were further characterized by the presence of potential hydrogen bonds, indicated by yellow dotted lines in the figure.

Detailed scoring of these interactions is provided in Table 1. The value of K_i is calculated from the Eq. (2), where K_i is the inhibition constant, Affinity is free energy of binding and the value given by AutoDock vina 1.1.2, R is the universal gas constant with a value of 0.00198179 kcal/(mol·K), and T is the temperature in Kelvin scale used in AutoDock vina 1.1.2 (298.15 K).The docking results indicated that the affinity of H_3RESCA-FAPI for the FAP protein was greater than that of DOTA-FAPI-04 and NOTA-FAPI-42.

$$K_i = e^{\frac{\text{affinity}}{RT}}, \tag{2}$$

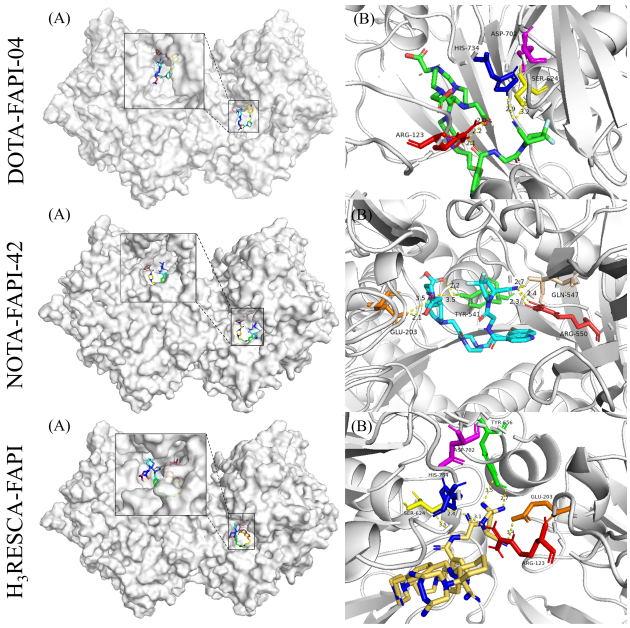

Fig. 2. Molecular modeling: (A) FAP ligand binding cavity of FAPIs and (B) Interaction diagram between amino acid residues of FAPIs and FAP in ligand binding pocket.

TABLE 1. Affinity score of the optimal conformation determined by molecular coupling (AutoDock vina 1.1.2), as well as the K_i and the distance from best mode (RMSD values).

Ligand	Affinity (kcal/mol)	K_i (nM)	rmsd 1.b.	rmsd u.b.
DOTA-FAPI-04	-9.1	204.85	0.000	0.000
NOTA-FAPI-42	-8.9	287.36	0.000	0.000
H_3RESCA	-10.0	44.66	0.000	0.000

B. ADMET Profiling Study

In the preliminary stages of Computer-Aided Drug Design (CADD), ADMET profiles of chemical compounds are acknowledged as critical factors. The pharmacokinetic properties and drug-likeness metrics for these compounds are detailed in Table S1, S2 and S3, respectively.

Pharmacokinetic analysis indicates that H_3RESCA-FAPI possesses a higher intestinal absorption (HIA) profile compared to DOTA-FAPI-04, which exhibits lower absorption rates. Both ligands demonstrated limited ability to cross the blood-brain barrier. The human colon epithelial cancer cell line, Caco-2, serves as a surrogate for studying drug intestinal absorption in humans. Permeability studies using the Caco-2

model revealed no significant difference between the two ligands in terms of membrane permeation. Additionally, drug-likeness was assessed based on the Lipinski Rule, Pfizer Rule, GSK Rule, and Golden Triangle Rule. Both compounds adhered to the Pfizer Rule; however, they did not comply with the Lipinski, GSK, and Golden Triangle criteria. For radioactive diagnostic agents, the administered doses are typically very low, thus mitigating concerns regarding the chemical toxicity of such drugs. In summary, the simulation experiments indicate that the two inhibitors are largely comparable, with the primary differences being their lipid solubility and intestinal uptake. The variance in lipid solubility may underlie the observed differences in intestinal absorption.

C. Binding Affinity

Surface plasmon resonance (SPR) was utilized to evaluate the interaction between DOTA-FAPI-04 and H_3RESCA-FAPI with recombinant human FAP protein (Fig. 3). The equilibrium dissociation constant (K_D) value of the 2 inhibitors binding to human FAP proteins exhibited a robust affinity, being in the picomole (pM) range. Specifically, The K_D value of DOTA-FAPI-04 is less than 27.89 pM, while The K_D value of H_3RESCA-FAPI is less than 10.09 pM (Fig. 3 (A) and (B)). This shows that the affinity of H_3RESCA-FAPI for FAP protein is slightly higher than that of DOTA-FAPI-04, which is consistent with the results of molecular docking simulation.

The molecular docking simulations and ADMET profiling study established the structural feasibility of H_3RESCA-FAPI, predicting its interactions with FAP and its pharmacokinetic properties. The high binding affinity of H_3RESCA-FAPI to FAP, as determined by SPR, is consistent with the docking results and underscores the potential of this tracer for specific targeting of FAP-expressing tumors.

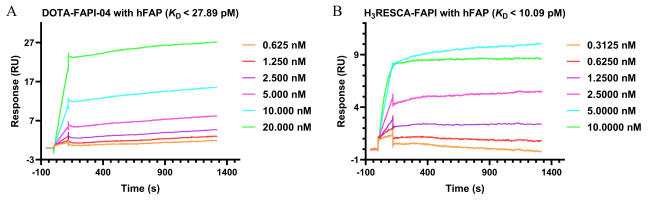

Fig. 3. (A) DOTA-FAPI-04 and (B) H_3RESCA reactive curves with recombinant human FAP protein.

D. Chemical and Radiochemical Syntheses

H_3RESCA-FAPI (compound 3) was synthesized (Fig. 4 (A)), and its molecular weight was identified by LC-MS (Fig. S1).

^{18}F-labeled FAP tracer was generated via the formation of complexes of Al^{18}F in a two-steps reaction. According to the lateral comparison, the reaction conditions with the highest labeling yield was as follows: buffer pH=5.0, the mole ratio of $AlCl_3$ to precursor was 0.58, and the weight of H_3RESCA-FAPI was 50 μg (Fig. 4 and Table S4). The highly reproducible radiolabeling yield of 95% was obtained in the optimal conditions.

Under the optimum labeling conditions, the total time needed for radiosynthesis was approximately 20 min, and the non-decay corrected radiochemistry yields (RCYs) of [^{18}F]AlF-H_3RESCA-FAPI was 52.0 $\pm$ 3.0% (n = 6). The radiochemical purity (RCP) of [^{18}F]AlF-H_3RESCA-FAPI was over 95% with molar activities of more than 14.5 GBq/μmol (n = 6) according to radioactivity measurements (Fig. 5 (A), S2 and S3). The labeling yield is not only related to the three factors screened (pH of buffer, the ratio of $AlCl_3$ to precursor and the dosage of precursor), but is also influenced by other factors (room temperature and the concentration of reaction solution), resulting in significant variability in labeling yields under identical conditions.

The radiochemical synthesis of [^{18}F]AlF-H_3RESCA-FAPI yielded a product with high RCP and RCYs, which is crucial for the practical application of the tracer in a clinical setting. The optimal conditions for radiolabeling, including pH, the molar ratio of aluminum chloride to precursor, and the mass of H_3RESCA, were identified, providing a reliable protocol for the production of the tracer. Considering that the pH value of colloidal $Al(OH)_3$ transformed from $AlCl_3$ is above 5.5 [24] and the labeling yield is unstable in the buffer with pH = 5.5, the buffer with pH = 5.0 is selected as the best condition. The capability of [^{18}F]AlF-H_3RESCA-FAPI to achieve high radiolabeling yields at room temperature is a critical advantage. It simplifies the synthesis process, reducing the need for complex and costly equipment typically required for heating reactions. This not only lowers the barriers to production but also increases the feasibility of translating this tracer into a clinical setting.

E. Octanol-Water Partition Coefficient and Stability Assay

The octanol-water partition coefficient, expressed as $\log D_{7.4}$, for the radiopharmaceuticals [^{68}Ga]Ga-DOTA-FAPI-04 and [^{18}F]AlF-H_3RESCA-FAPI were calculated to be -3.53 $\pm$ 0.05 and -2.47 $\pm$ 0.16, respectively. This comparative analysis suggests that [^{18}F]AlF-H_3RESCA-FAPI possesses a reduced hydrophilicity in comparison to [^{68}Ga]Ga-DOTA-FAPI-04. Given the constraints inherent in the ADMETLab 3.0 regarding the processing of SMILES files that include metal complexes, the distribution coefficients of the respective uncomplexed precursors served as a benchmark for assessing the hydrophilicity of these radiopharmaceutical agents (the logP of DOTA-FAPI-04 and H_3RESCA-FAPI are -1.982 and -0.639, respectively). The observed hydrophilicity trends corroborate the simulation results obtained for the labeled precursors during ADMET prediction analyses. It demonstrated that [^{18}F]AlF-H_3RESCA-FAPI has reduced hydrophilicity compared to [^{68}Ga]Ga-DOTA-FAPI-04, which may influence its biodistribution and pharmacokinetics.

Furthermore, the stability assessment of [^{18}F]AlF-H_3RESCA-FAPI in phosphate-buffered saline (PBS,

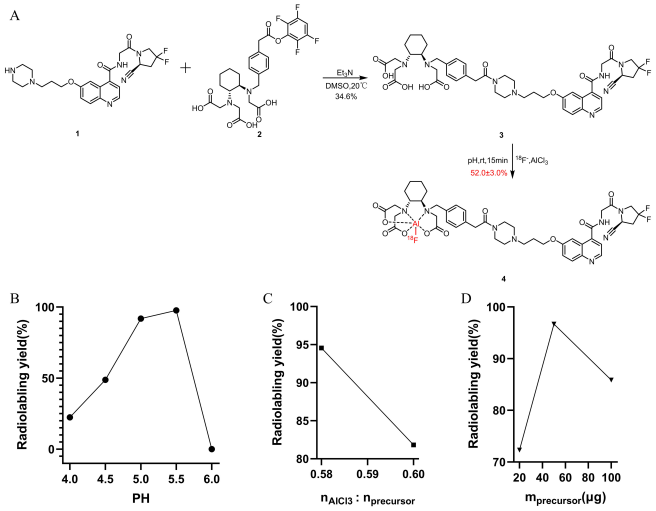

Fig. 4. Synthesis of [^{18}F]AlF-H$_3$RESCA-FAPI (A); Labeling yield of [^{18}F]AlF-H$_3$RESCA-FAPI under different reaction conditions. Labeling yield under different pH values (4.0, 4.5, 5.0, 5.5, 6.0) of buffer system (B); The labeling yield was fixed (20 μg) with different $AlCl_3$-ligand ratios (0.58, 0.60) (C); The ligand ratio of $AlCl_3$ is fixed (the molar ratio of substances is 0.58), and the labeling yield is different under different ligand mass (20 μg, 50 μg, 100 μg) (D).

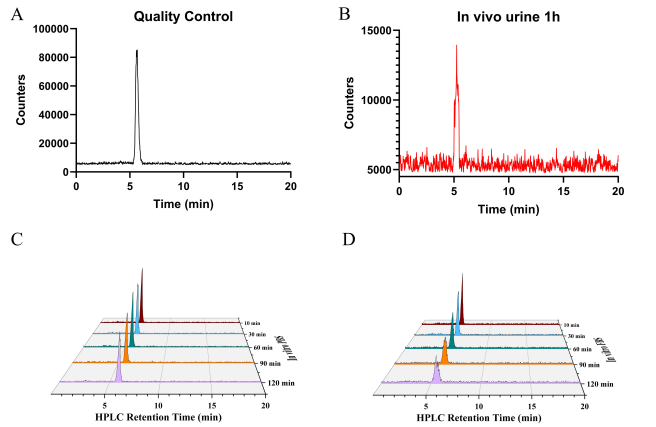

Fig. 5. Representative HPLC graphs of quality control of [^{18}F]AlF-H$_3$RESCA-FAPI (A), *in vivo* metabolism study of [^{18}F]AlF-H$_3$RESCA-FAPI at 1 hour after injection (B) and its stability at 37°C for 2 hours in PBS (C) and FBS (D).

pH=7.4), fetal bovine serum (FBS), and mouse urine—presented in Fig. 5, underscores the tracer's robust stability in both *in vitro* and *in vivo* conditions.

F. Plasma Clearance

The Plasma Clearance experiment involved the collection of blood drug concentration (%ID/g) at specific time points and fitting a curve to the data. The distribution-phase half-life ($t_{1/2\alpha}$) value of the [^{18}F]AlF-H$_3$RESCA-FAPI was 0.76 min, and its clear-phase half-life ($t_{1/2\beta}$) value was more than 60 min (Fig. 6 and Table S5). The plasma clearance data revealed a rapid distribution phase and a longer clearance phase, suggesting that the tracer is rapidly taken up by tissues and slowly cleared from the body.

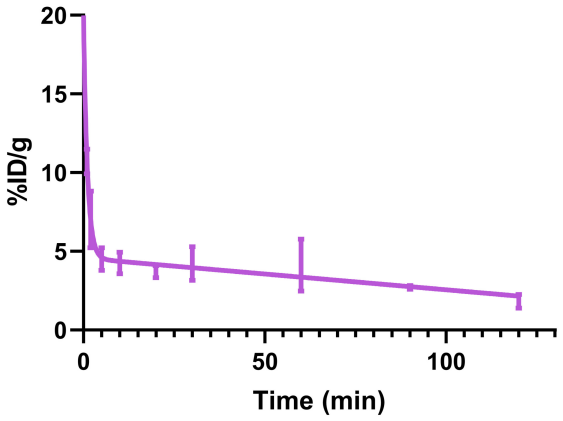

Fig. 6. Activity curve: blood drug concentration of [^{18}F]AlF-H$_3$RESCA-FAPI (n = 3).

G. PET/CT Imaging

Static PET imaging studies were performed in U87MG tumor-bearing nude mice to investigate the pharmacokinetics of [^{18}F]AlF-H$_3$RESCA-FAPI. The coronal and axial images of [^{18}F]AlF-H$_3$RESCA-FAPI at different scanning times are shown in Fig. 7 (A). The tissue accumulation of tracer is described by standardized uptake value (SUV) scale. With regard to tumors, [^{18}F]AlF-H$_3$RESCA-FAPI accumulated rapidly in U87MG tumor xenografts. A slow increase in tumor uptake was observed from 10 to 120 min (SUVmax, from 0.70 $\pm$ 0.02 to 0.72 $\pm$ 0.06). This observation indicates that [^{18}F]AlF-H$_3$RESCA-FAPI exhibits a considerable retention time within the tumor.

However, the liver and intestine exhibited significantly uptake values, possibly due to the certain lipid solubility of the tracer. Both ADMET prediction and $LogD_{7.4}$ measurement support this and predict increased intestinal absorption. In U87MG tumor model mice, from 10 to 120 min, [^{18}F]AlF-H$_3$RESCA-FAPI demonstrated rapid clearance kinetics in muscle (SUVmax, from 0.029 $\pm$ 0.002 to 0.014 $\pm$ 0.002), intestine (SUVmax, from 139.092 $\pm$ 43.447 to 53.872 $\pm$ 27.220) and liver (SUVmax, from 2.251 $\pm$ 0.539 to 1.403 $\pm$ 0.370), while clearance from the kidney was comparatively slower. The relatively low uptake of [^{18}F]AlF-H$_3$RESCA-FAPI in the kidney resulted in less noticeable numerical changes (SUVmax, less than 0.10), whereas the significantly high uptake in the intestine (SUVmax, more than 15.60) led to more pronounced numerical changes. It requires further validation to determine whether the observed uptake value in the intestine is attributable to direct absorp-

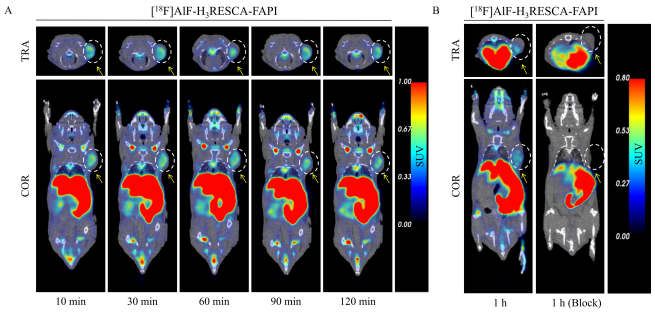

Fig. 7. (A) Representative static PET images of [^{18}F]AlF-H_3RESCA-FAPI in U87MG xenograft models at different time points. (B) Representative static PET images of [^{18}F]AlF-H_3RESCA-FAPI in U87MG xenograft models with simultaneous injection of unlabeled DOTA-FAPI-04 as a competitor at 60 min. The yellow arrows point to the tumor.

tion within the intestinal tissue or to metabolites generated by the radioactive tracer that subsequently enter the intestine through metabolic pathways. The results of the blocking experiment, depicted in Fig. 7 (B), demonstrate a successful reduction in tumor uptake following co-administration of unlabeled DOTA-FAPI-04 (SUVmax, unblocking vs. blocking at 1h, 0.49 $\pm$ 0.18 vs. 0.04 $\pm$ 0.02, P = 0.0124). Moreover, significant reductions in uptake values were observed in the liver and bone.

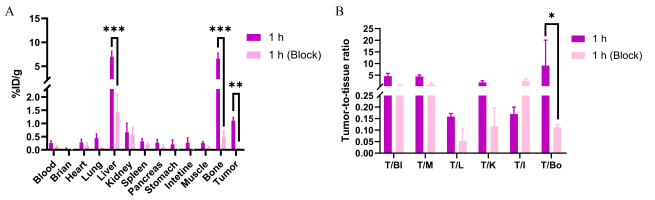

Fig. 8. The *ex vivo* Biodistribution of [^{18}F]AlF-H_3RESCA-FAPI in U87MG model mice 1 hour after injection (A) and the uptake ratio of [^{18}F]AlF-H_3RESCA-FAPI in tumor and blood, muscle, liver, kidney, intestine, bone (B) were co-administered with and without unlabeled DOTA-FAPI-04 as a blocking agent. All the data are expressed as mean $\pm$ SD values, n = 3.

PET/CT imaging and biodistribution studies in U87MG tumor-bearing mice showed specific and significant uptake of [^{18}F]AlF-H_3RESCA-FAPI in tumors, with high tumor-to-background ratios, indicating its potential for accurate tumor imaging. The high bone uptake observed is a common characteristic of ^{18}F-labeled tracers [25–35]. The significant reduction in tumor uptake following co-administration of unlabeled DOTA-FAPI-04 further confirms the specificity of [^{18}F]AlF-H_3RESCA-FAPI for FAP-expressing tumors.

H. Biodistribution

Further biodistribution experiments of tumor-bearing mice were performed to validate the findings from PET imaging. The results indicated a significant uptake of [^{18}F]AlF-H_3RESCA-FAPI in the liver, where it is primarily metabolized. In Comparison to the image results obtained from PET, the primary distinction lies in the reduced intestinal uptake (Fig. 8 and Table 2). This reduction can be attributed to the elimination of metabolites from the organs during the collection process, thereby demonstrating the rapid metabolism of [^{18}F]AlF-H_3RESCA-FAPI in the liver and intestines. Apart from this difference, the imaging results are largely consistent with those of PET.

TABLE 2. Biodistribution data of [^{18}F]AlF-H_3RESCA-FAPI co-injected with competitor DOTA-FAPI-04 (0.5 mg/mouse, blocking) in U87MG xenografts female mice (n = 3) for 60 min p.i. and selected organ of biodistribution in U87MG xenografts model mice (n = 3) administered with [^{18}F]AlF-H_3RESCA-FAPI for 60 min p.i (%ID/g).

	60 min	60 min blocking
Blood	0.25 $\pm$ 0.08	0.20 $\pm$ 0.04
Brain	0.03 $\pm$ 0.03	0.01 $\pm$ 0.00
Heart	0.27 $\pm$ 0.13	0.14 $\pm$ 0.12
Lung	0.44 $\pm$ 0.16	0.06 $\pm$ 0.03
Liver	6.99 $\pm$ 1.18	1.43 $\pm$ 0.70
Kidney	0.66 $\pm$ 0.34	0.58 $\pm$ 0.29
Spleen	0.32 $\pm$ 0.10	0.20 $\pm$ 0.07
Pancreas	0.26 $\pm$ 0.13	0.09 $\pm$ 0.08
Stomach	0.20 $\pm$ 0.17	0.02 $\pm$ 0.01
Intestine	0.27 $\pm$ 0.19	0.02 $\pm$ 0.00
Muscle	0.26 $\pm$ 0.06	0.07 $\pm$ 0.05
Bone	6.60 $\pm$ 1.16	0.49 $\pm$ 0.23
Tumor	1.10 $\pm$ 0.12	0.05 $\pm$ 0.02

The uptake of [^{18}F]AlF-H_3RESCA-FAPI in tumor was 1.10 $\pm$ 0.12 %ID/g, which decreased to 0.05 $\pm$ 0.02 %ID/g after blocking, indicating a high level of specific uptake in tumor (P = 0.004). Additionally, the tracer demonstrated significant tumor-muscle and tumor-blood ratios of 4.40 $\pm$ 0.71 and 4.56 $\pm$ 1.18, respectively. The substantial bone uptake of most ^{18}F-labeled tracers remains evident, with the uptake quantified at 6.60 $\pm$ 1.16 %ID/g, which decreased to 0.49 $\pm$ 0.23 %ID/g after blocking (P $<$ 0.001). Notwithstanding this characteristic, [^{18}F]AlF-H_3RESCA-FAPI demonstrates considerable promise as a PET tracer specifically targeting FAP.

I. Immunohistochemical Staining

The tumor of U87MG model mice was cut and soaked in formalin solution, and the staining pattern of FAP was obtained after immunohistochemical staining experiment, which confirmed that all animal experiments of this tracer were carried out in animal models with FAP expression (Fig. 9).

IV. SUMMARY

In this study, a novel radiopharmaceutical, [^{18}F]AlF-H_3RESCA-FAPI, was synthesized utilizing the established

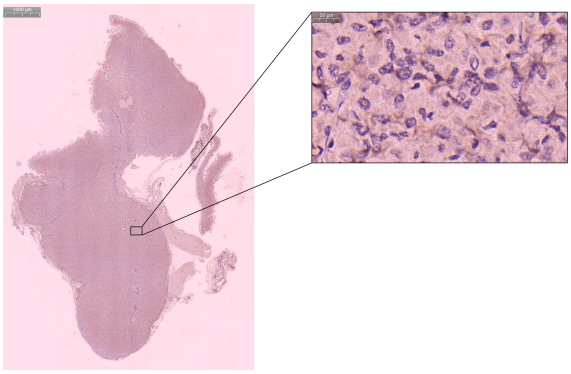

Fig. 9. Immunohistochemical staining of FAP expression in U87MG tumor tissues.

FAPI scaffold. In comparison to existing FAPI-based tracers, [^{18}F]AlF-H_3RESCA-FAPI demonstrates improved labeling-method, which is a significant advancement. It was evaluated *in vitro* and *in vivo*, and showed considerable specific uptake of FAP-expressing tumors in mice. It exhibited a extremely mild labeling process and high specificity. Therefore, this novel FAP-targeted radioactive tracer may be a promising tracer for non-invasive tumor imaging in subsequent clinical research, but its structure needs to be further modified to obtain better pharmacokinetic characteristics.

[1] X. Chen, E. Song, Turning foes to friends: targeting cancer-associated fibroblasts. Nat. Rev. Drug. Discov. **18**, 99–115 (2018). doi: 10.1038/s41573-018-0004-1

[2] E. Puré, R. Blomberg, Pro-tumorigenic roles of fibroblast activation protein in cancer: back to the basics. Oncogene. **37**, 4343–4357 (2018). doi: 10.1038/s41388-018-0275-3

[3] T. Lindner, A. Loktev, F. Giesel et al., Targeting of activated fibroblasts for imaging and therapy. EJNMMI. Radiopharm. Chem. **4**, 1415–1422 (2019). doi: 10.1186/s41181-019-0069-0

[4] E.J. Hamson, F.M. Keane, S. Tholen et al., Understanding fibroblast activation protein (FAP): substrates, activities, expression and targeting for cancer therapy. Proteomics. Clin. Appl. **8**, 454–463 (2014). doi: 10.1002/prca.201300095

[5] S. Lamprecht, I. Sigal-Batikoff, S. Shany et al., Teaming up for trouble: cancer cells, transforming growth factor-β1 signaling and the epigenetic corruption of stromal naïve fibroblasts. Cancers. **10**, 10030061 (2018). doi: 10.3390/cancers10030061

[6] L. Bu, H. Baba, N. Yoshida et al., Biological heterogeneity and versatility of cancer-associated fibroblasts in the tumor microenvironment. Oncogene. **38**, 4887–4901 (2019). doi: 10.1038/s41388-019-0765-y

[7] P. Busek, R. Mateu, M. Zubal et al., Targeting fibroblast activation protein in cancer – Prospects and caveats. Front. Biosci. (Landmark Ed) **23**, 1933–1968 (2018). doi: 10.2741/4682

[8] A. Šimková, P. Bušek, A. Šedo et al., Molecular recognition of fibroblast activation protein for diagnostic and therapeutic applications. Biochim. Biophys. Acta. Proteins. Proteomics. **1868**, 140409 (2020). doi: 10.1016/j.bbapap.2020.140409

[9] K. Jansen, L. Heirbaut, R. Verkerk et al., Extended structure–activity relationship and pharmacokinetic investigation of (4-quinolinoyl)glycyl-2-cyanopyrrolidine inhibitors of fibroblast activation protein (FAP). J. Med. Chem. **57**, 3053–3074 (2014). doi: 10.1021/jm500031w

[10] K. Jansen, L. Heirbaut, J. Cheng et al., Selective inhibitors of fibroblast activation protein (fap) with a (4-quinolinoyl)-glycyl-2-cyanopyrrolidine scaffold. ACS. Med. Chem. Lett. **4**, 491–496 (2013). doi: 10.1021/ml300410d

[11] T. Lindner, A. Loktev, A. Altmann et al., Development of quinoline-based theranostic ligands for the targeting of fibroblast activation protein. J. Nucl. Med. **59**, 1415–1422 (2018). doi: 10.2967/jnumed.118.210443

[12] A. Loktev, T. Lindner, W. Mier et al., A tumor-imaging method targeting cancer-associated fibroblasts. J. Nucl. Med. **59**, 1423–1429 (2018). doi: 10.2967/jnumed.118.210435

[13] A. Loktev, T. Lindner, E.-M. Burger et al., Development of fibroblast activation protein–targeted radiotracers with improved tumor retention. J. Nucl. Med. **60**, 1421–1429 (2019). doi: 10.2967/jnumed.118.224469

[14] C. Kratochwil, P. Flechsig, T. Lindner et al., ^{68}Ga-FAPI PET/CT: tracer uptake in 28 different kinds of cancer. J. Nucl. Med. **60**, 801–805 (2019). doi: 10.2967/jnumed.119.227967

[15] N. Zhang, F. Pan, L. Pan et al., Synthesis, radiolabeling, and evaluation of a (4-quinolinoyl)glycyl-2-cyanopyrrolidine analogue for fibroblast activation protein (FAP) PET imaging. Front. Bioeng. Biotechnol. **11**, 1167329 (2023). doi: 10.3389/fbioe.2023.1167329

[16] Z.H. Cho, J.K. Chan, L. Ericksson et al., Positron ranges obtained from biomedically important positron-emitting radionuclides. Journal of nuclear medicine: official publication, Soc. Nucl. Med. **16**, 1174-1176 (1975). doi: content/16/12/1174.long

[17] K. Hu, J. Li, L. Wang et al., Preclinical evaluation and pilot clinical study of [^{18}F]AlF-labeled FAPI-tracer for PET imaging of cancer associated fibroblasts. Acta. Pharm. Sin. B **12**, 867–875 (2022). doi: 10.1016/j.apsb.2021.09.032

[18] Z. Yu, Y. Huang, H. Chen et al., Design, synthesis, and evaluation of ^{18}F-labeled tracers targeting fibroblast activation protein for brain imaging. ACS. Pharmacol. Transl. Sci. **6**, 1745–1757 (2023). doi: 10.1021/acsptsci.3c00187

[19] J. Toms, J. Kogler, S. Maschauer et al., Targeting fibroblast activation protein: radiosynthesis and preclinical evaluation of an ^{18}F-labeled fap inhibitor. J. Nucl. Med. **61**, 1806–1813 (2020). DOI: 10.2967/jnumed.120.242958

[20] H. Zhou, J. Zhong, S. Peng et al., Synthesis and preclinical evaluation of novel ^{18}F-labeled fibroblast activation protein tracers for positron emission tomography imaging of cancer-associated fibroblasts. Eur. J. Med. Chem **264**, 115993 (2024). doi: 10.1016/j.ejmech.2023.115993

[21] L. Carroll, D. Holt, H. Cha, et al., Investigating the mechanism of aluminum fluoride chelation. Inorg. Chem. **63**, 9831–9841 (2024). doi: 10.1021/acs.inorgchem.4c00400

[22] F. Cleeren, J. Lecina, J. Bridoux et al., Direct fluorine-18 labeling of heat-sensitive biomolecules for positron emission tomography imaging using the Al^{18}F-RESCA method. Nat. Protoc. **13**, 2330–2347 (2018). doi: 10.1038/s41596-018-0040-7

[23] O. Wegrzyniak, F. Lechi, B. Mitran et al., Non-invasive PET imaging of liver fibrogenesis using a RESCA-conjugated affibody molecule. iScience. **27**, 109688 (2024). doi: 10.1016/j.isci.2024.109688

[24] X. Wang, H. Xu, D. Wang et al., Mechanism of fluoride removal by $AlCl_3$ and AlI_3: The role of aluminum speciation. J. Hazard. Mater. **398**, 122987 (2020). doi: 10.1016/j.jhazmat.2020.122987

[25] X. Chen, D. Xia, X. Zeng et al., Rational design and pharmacomodulation of ^{18}F-labeled biotin/FAPI-conjugated heterodimers. J. Med. Chem. **67**, 8361–8371 (2024). doi: 10.1021/acs.jmedchem.4c00544

[26] L. Liu, J. Zhong, Z. Zhang et al., Preclinical study and first-in-human imaging of [^{18}F]FAP-2286, and comparison with 2-[^{18}F]FDG PET/CT in various cancer patients. Eur. J. Nucl. Med. Mol. Imaging. **51**, 2012–2022 (2024). doi: 10.1007/s00259-024-06626-9

[27] A. Craig, J. Kogler, M. Laube et al., Preparation of ^{18}F-labeled tracers targeting fibroblast activation protein via sulfur [^{18}F]fluoride exchange reaction. Pharmaceutics. **15**, 15122749 (2023). doi: 10.3390/pharmaceutics15122749

[28] X. Zhang, J.Y. Choi, K.-H. Lee et al., Synthesis and evaluation of [^{18}F]SiFA-conjugated ligands for fibroblast activation protein imaging. Mol. Pharmaceutics. **20**, 6441–6450 (2023). doi: 10.1021/acs.molpharmaceut.3c00824

[29] C.B.M Poulie, V. Shalgunov, F. Elvas et al., Next generation fibroblast activation protein (FAP) targeting PET tracers - The tetrazine ligation allows an easy and convenient way to ^{18}F-labeled (4-quinolinoyl)glycyl-2-cyanopyrrolidines. Eur. J. Nucl. Med. **262**, 115862 (2023). doi: 10.1016/j.ejmech.2023.115862

[30] L. Fu, J. Huabf, Q. Liu et al., Radiosynthesis, preclinical evaluation and pilot clinical PET imaging study of a ^{18}F-labeled tracer targeting fibroblast activation protein. Bioorganic. Chem. **141**, 106878 (2023). doi: 10.1016/j.bioorg.2023.106878

[31] J. Huang, L. Fu, X. Zhang et al., Noninvasive imaging of FAP expression using positron emission tomography: A comparative evaluation of a [^{18}F]-labeled glycopeptide-containing FAPI with [^{18}F]FAPI-42. Eur. J. Nucl. Med. Mol. Imaging. **50**, 3363–3374 (2023).doi: 10.1007/s00259-023-06282-5

[32] X. Li, J. Ye, J. Wang et al., First-in-humans PET imaging of KRASG12C mutation status in non–small cell lung and colorectal cancer patients using [^{18}F]PFPMD. J. Nucl. Med. **64**, 1880–1888 (2023). doi: 10.2967/jnumed.123.265715

[33] T. Yang, L. Peng, J. Qiu et al., A radiohybrid theranostics ligand labeled with fluorine-18 and lutetium-177 for fibroblast activation protein-targeted imaging and radionuclide therapy. Eur. J. Nucl. Med. Mol. Imaging. **50**, 2331–2341 (2023). doi: 10.1007/s00259-023-06169-5

[34] Z. Wang, B. Zhu, F. Jiang et al., Design, synthesis and evaluation of novel prostate-specific membrane antigen-targeted aryl [^{18}F]fluorosulfate PET tracers. Bioorg. Med. Chem. **106**, 117753 (2024). doi: 10.1016/j.bmc.2024.117753

[35] F. Francis, M. Wuest, J.D. Woodfield et al., Palladium-mediated s-arylation of cysteine residues with 4-[^{18}F]Fluoroiodobenzene ([^{18}F]FIB). Bioconjug. Chem. **35**, 232–244 (2024). doi: 10.1021/acs.bioconjchem.3c00522